Geofísica Internacional (2025) **64-1**: 1367 - 1378

Detection of ionospheric response to earthquakes in Mexico: case study of September 8, 2021 and September 19, 2022

Angela Melgarejo-Morales[1], Maria A. Sergeeva[1,2]*, Ekaterina Kazachkina[3], Artem M. Vesnin[4] and Ernesto Aguilar-Rodriguez[1]

Abstract

We explore the possibility of the ionospheric disturbance detection after two earthquakes (EQ) (M_w > 7) occurred on September 8, 2021, and September 19, 2022, in Mexico. The epicenter location, depth, focal mechanism, season and Space Weather background conditions were similar for the two EQs. The local time and the magnitude were different. Wave responses in the filtered slant TEC time series were revealed after both EQs at isolated satellite-receiver ray paths. The irregular variations exceeded the background fluctuation level and were not repeated on other days. Their form and temporal scales allowed us to associate them with the acoustic-gravity waves generated by the vertical displacement during the powerful EQs. The nighttime EQ on September 8, 2021, caused the medium-scale disturbances characterized with the N- and И-form fluctuations in TEC, a period of ~30 min and amplitudes of (0.1-0.2) TECU. The response to the daytime EQ on September 19, 2022, was of two types: small-scale disturbances N-, V-, И- and M-form with a 15 min period and amplitudes of (0.1-1.1) TECU; and medium-scale disturbances of N- and И-form with a period of ~30 min and amplitudes of (0.1-0.2) TECU. The presented conclusions for the Mexican region are preliminary as more statistics are needed.

Key words: co-seismic ionospheric disturbance, earthquakes, slant TEC, Mexico.

Resumen

Exploramos la posibilidad de detectar perturbaciones ionosféricas después de dos terremotos (EQ) (M_w > 7) registrados el 8 de septiembre de 2021 y el 19 de septiembre de 2022 en México. La ubicación del epicentro, la profundidad, el mecanismo focal, la estación del año y las condiciones de fondo del Clima Espacial fueron similares para los dos EQ. La hora local y la magnitud fueron diferentes. Se observaron respuestas, en forma de ondas, en la serie temporal de TEC inclinado filtrado, después de ambos EQ, en trayectorias de rayos aislados entre satélites y receptores. Las variaciones irregulares superaron el nivel de fluctuación de fondo y no se repitieron en otros días. Su forma y escalas temporales permitieron asociarlas con las ondas acústicas-gravitacionales generadas por el desplazamiento vertical durante los poderosos EQ. El EQ nocturno del 8 de septiembre causó perturbaciones a escala media, caracterizadas por fluctuaciones de forma N y И en TEC, con un período de ~30 min y amplitudes de (0.1-0.2) TECU. La respuesta al EQ diurno del 19 de septiembre fue de dos tipos: perturbaciones a escala pequeña de forma N y И, con un período de ~15 min y amplitudes de (0.1-1.1) TECU; y perturbaciones a escala media de forma N, V, И y M, con un período de ~30 min y amplitudes de (0.1-0.2) TECU. Las conclusiones presentadas para la región mexicana son preliminares, ya que se necesitan más datos estadísticos.

Palabras clave: perturbaciones ionosféricas co-sísmicas, terremotos, TEC oblicuo, México.

Received: January 10, 2024; Accepted: August 24, 2024; Published on-line: January 1, 2025.

Editorial responsibility: Dra. Inez Staciarini-Batista

* Corresponding author: Maria A. Sergeeva, maria.a.sergeeva@gmail.com.
[1] SCiESMEX, LANCE, Instituto de Geofísica, Unidad Michoacán, Universidad Nacional Autónoma de México, México.
[2] CONAHCYT, Instituto de Geofísica, Unidad Michoacán, Universidad Nacional Autónoma de México, México.
[3] Instituto de Geofísica, Universidad Nacional Autónoma de México, México.
[4] Institute of Solar-Terrestrial Physics, Siberian Branch of Russian Academy of Sciences, Irkutsk, Russia.

Angela Melgarejo-Morales, Maria A. Sergeeva, Ekaterina Kazachkina, Artem M. Vesnin, Ernesto Aguilar-Rodríguez
https://doi.org/10.22201/igeof.2954436xe.2025.64.1.1774

1. Introduction

The ionospheric response to seismic events has been a subject of the scientific interest over the recent decades. Several authors have addressed the ionospheric disturbances related to earthquakes that occurred in different regions, for example (Davies and Baker, 1965; Calais and Minster, 1995; Afraimovich *et al.*, 2001; Ducic *et al.*, 2003; Heki and Ping, 2005; Afraimovich *et al.*, 2006; Lognonné et el., 2006; Liu *et al.*, 2010; Astafyeva *et al.*, 2009; Jin *et al.*, 2015; Kong *et al.*, 2018; Oikonomou *et al.*, 2020; Melgarejo-Morales *et al.*, 2023; Bravo *et al.*, 2022) and many others. Ionospheric disturbances that occur after earthquakes are commonly referred to as Co-seismic Ionospheric Disturbances (CIDs). These disturbances are primarily attributed to the release of energy during earthquakes, a process capable of generating atmospheric waves that propagate upwards into the ionosphere.

The ionosphere is known to respond to changes in Space Weather conditions, explosions of different type, tropical cyclones, hurricanes and others, for example (Afraimovich *et al.*, 2013; Perevalova *et al.*, 2015; Perevalova and Ishin, 2011). The difficulty for CID studies is that the signatures of ionospheric disturbances caused by an earthquake can be similar to those caused by some other natural phenomena. This fact underscores the complexity of this research domain. The mechanisms triggering CIDs comprise direct acoustic waves caused by vertical crustal movements or sea surface interactions, Rayleigh surface waves, and internal gravity waves. As these atmospheric waves ascend to the F region of the ionosphere, they can induce irregularities in the electron concentration. The latter can be detected as Travelling Ionospheric disturbances (TIDs). For more details on the physical mechanisms of the described processes, the reader is referred to comprehensive reviews (Astafyeva, 2019; Afraimovich *et al.*, 2013; Hocke and Schlegel, 1996).

There are gaps in our understanding on the particular features of CIDs in different regions, their spatiotemporal scales, movement speeds, and even their occurrence or non-occurrence in different latitudinal and longitudinal sectors. The ionospheric response to seismic events depends on the earthquake magnitude (M_w) and regional geophysical conditions. Literature suggests that earthquakes with magnitudes exceeding $M_w > 6.5$ are more likely to trigger ionospheric responses, e.g. (Perevalova *et al.*, 2014 and references therein).

The aim of this work was to search for the ionospheric response to two particular earthquake (EQ) events that occurred in the low-latitude North-American region (south of Mexico) using Global Navigation Satellite System (GNSS) data. The tasks were to characterize the ionospheric responses if detected and compare them for the two chosen events. This paper is organized as follows. Section 2 introduces the data and method used for the study. Section 3 provides a description of the considered EQs. Section 4 describes the background conditions in the ionosphere. Section 5 presents the results of the ionospheric disturbances detection. Final remarks are given in Conclusions.

2. Data and method used

GNSS receiver data was obtained from two receiver networks: the "Transboundary, Land and Atmosphere Long-term Observational and Collaborative network (TLALOCNet)" at Servicio de Geodesia Satelital (Cabral-Cano *et al.*, 2018) and the "Servicio Sismológico Nacional" (Pérez-Campos *et al.*, 2018), both hosted at the Instituto de Geofísica, Universidad Nacional Autónoma de México. The location of the stations whose data was used in the present study is illustrated in Figure 1. It should be noted that the dataset used in this work is not extensive, primarily due to the uneven station distribution across the Mexican region. Nevertheless, the following analysis showed that these data allowed us to make at least rough assessments of the CIDs in the chosen region.

The "classical" approach for detecting the ionospheric response to EQ is to study slant Total Electron Content (TEC) variations along the Lines-of-Sight (LoSs) between GNSS satellites and receivers whose configuration corresponds to the area of interest. Usually, TEC time series are subjected to some filtering procedure designed to detect the specific form of TEC times series. Previous studies demonstrated that the compression-rarefaction N-wave, the inverse N-form (И) and wave-packet patterns can be detected in TEC variations associated with EQ (Liu *et al.*, 2010; Afraimovich *et al.*, 2013; Sripathi *et al.*, 2020; Shi *et al.*, 2020; Zhang *et al.*, 2021; Astafyeva, 2019; Rolland *et al.*, 2013).

Data of dual-frequency phase GNSS measurements was used to calculate TEC values along the different LoSs. Using the method described in (Yasukevich *et al.*, 2020), the obtained TEC time series were detrended with splines and filtered with the centered moving average. Two specific combinations of window sizes were chosen for this purpose, consisting of 2 and 10 minutes, as well as 10 and 20 minutes. The filtered TEC variations were then converted into equivalent vertical variations, denoted as (2-10)dI and (10-20)dI, correspondingly. The purpose was to have variation with periods in these ranges, as they correspond to different spatiotemporal scales of ionospheric disturbances.

A similar approach was successfully applied in the Mexican region for detecting the ionospheric responses to the meteoroid passage and explosion (Sergeeva *et al.*, 2021) and to the intense solar flares (Sergeeva *et al.*, 2023). It should be noted that the mechanism of transporting the energy released during EQs and during some explosion in the lower atmosphere such as the meteoroid explosion is basically the same. It is based on the

concept of the atmospheric waves propagating from below to the ionospheric heights while increasing the waves' amplitude (Afraimovich *et al.*, 2013).

In the present work, we analyzed the dI series during the time interval from 30 min before the seismic event (main shock) and 3.5 hours after it. To ascertain that dI responses if detected were not attributed to the multipath effect, the dI variations on the EQ day were compared to the same variations on the previous day. The fact that the same form of the dI curve is repeated from day to day, and is slightly shifted in time, indicates the presence of multipath effects.

3. Event description

In this work, we considered two seismic events with M_w more than 7 which occurred in the south of Mexico. The Mexican region is exposed to different natural hazards, such as hurricanes, volcanoes, earthquakes, tsunamis, etc. (Cabral-Cano *et al.*, 2018; Gonzalez-Esparza et al 2018; Sergeeva *et al.*, 2021). Sometimes, they even occur simultaneously representing a significant danger (Gonzalez-Esparza et al 2018). Mexico is located in an area of interaction of five tectonic plates: North American plate, Cocos plate, Pacific plate, Rivera plate and the Caribbean plate, which is the reason of high seismicity in the region (Figure 2). The seismic activity is frequent in the south of the country. This study is focused on two particular events that occurred in September 2021 and September 2022. Both EQ were the result of the interaction between the Cocos and North American plates.

The National Seismological Service reported the EQ of M_w 7.1 that occurred 11 km southwest of Acapulco, in the state of Guerrero on September 8th, 2021 at 01:47 UT (September 7th, 2021 at 20:47 central Mexican time) (SSN, 2021). Figure 2 shows its epicenter location. This EQ is associated with the plate boundary, where the oceanic Cocos plate subducts under the continental North American plate. The EQ rupture length reaches 30 km (United States Geological Servey (USGS), **https://earthquake.usgs.gov/earthquakes/eventpage/us7000f93v/executive)** and has a propagation directivity towards northeast (Iglesias *et al.*, 2022).

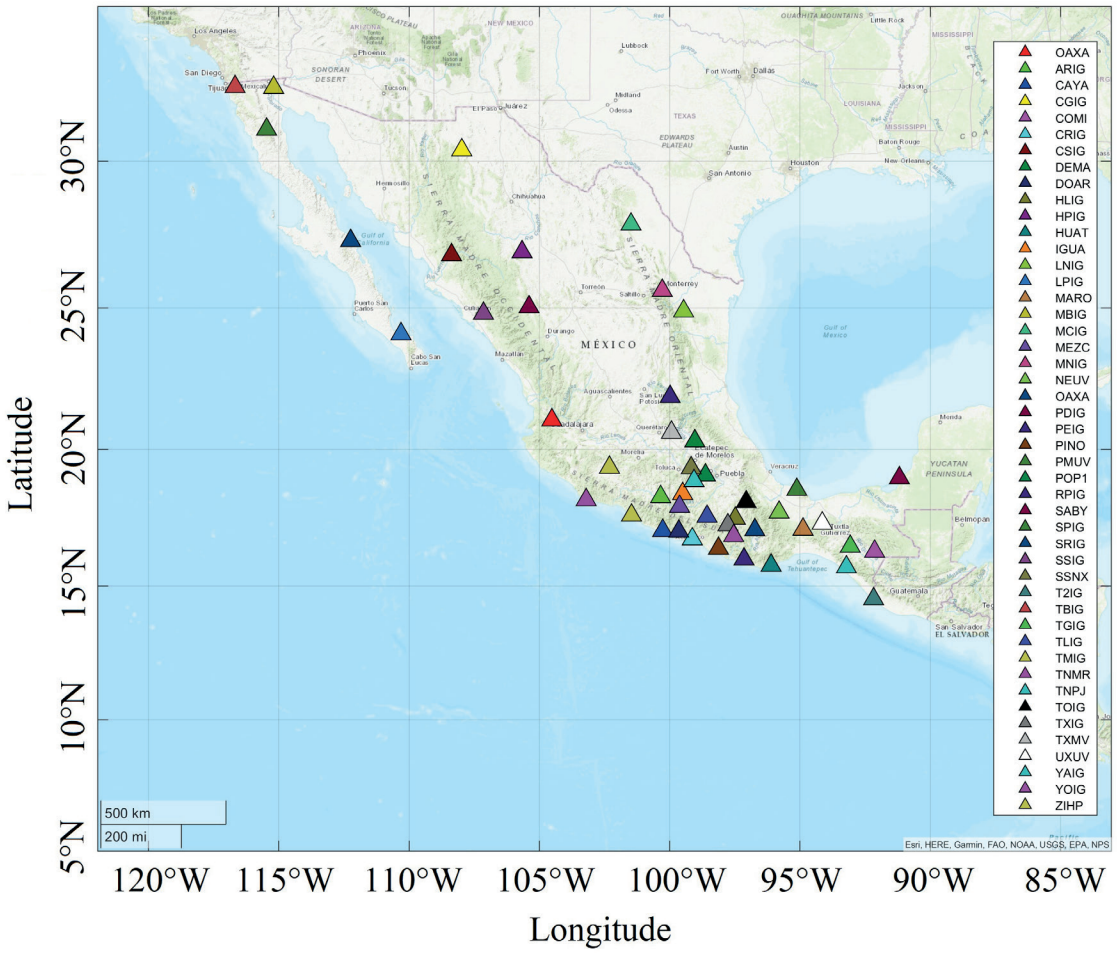

Figure 1. GNSS stations in the Mexican region.

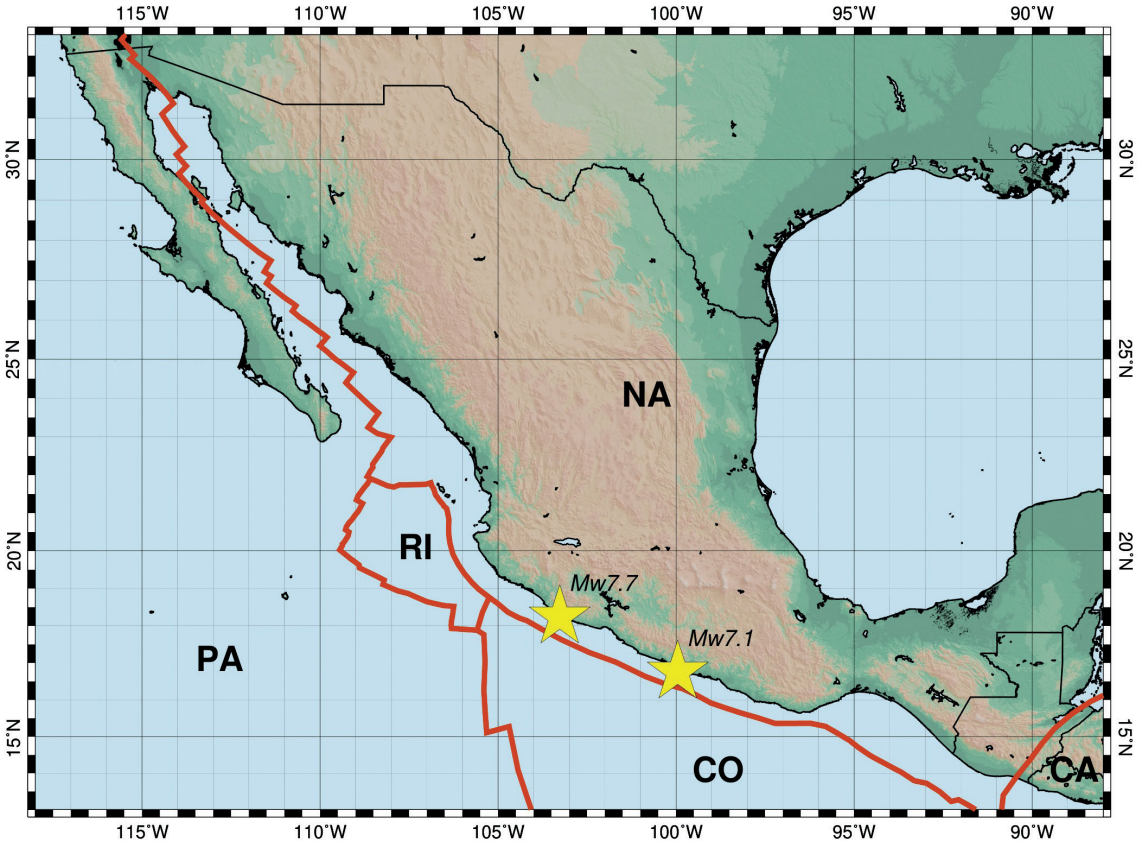

Figure 2. Tectonic plates in the region with EQ epicenter locations. Yellow stars mark the epicenter of the September 8, 2021, Mw7.1 and the September 19, 2022, Mw 7.7 seismic events. Tectonic plate names: NA – North American, PA – Pacific, RI – Rivera, CO – Cocos, CA – Caribbean.

The M_w 7.7 earthquake occurred on September 19th, 2022, at 18:05 (at 13:05 central Mexican time) near Coalcomán, in the state of Michoacán (Figure 2) (SSN, 2022). This EQ took place at the Cocos-North American plate interface. The rupture propagated towards northwest (Singh *et al.*, 2023). Table 1 shows the parameters of the two events. The reader is referred to the works (Iglesias *et al.*, 2022, Liu *et al.*, 2023; Ramírez-Rojas *et al.*, 2023, Singh *et al.*, 2023) for a more detailed description of the events.

Daytime and nighttime ionosphere is characterized by different values of electron density, temperature, physical processes, etc. (Davies and Baker, 1965; Kelly, 2009; Cander, 2019). In this work, we search for the ionospheric response to one EQ that occurred at local evening hours (almost night) and another that occurred after the midday (daytime conditions). The seasonal background conditions were practically the same since both events occurred in September. At the same time, the first EQ occurred during the low solar activity period, and the second EQ at the ascending part of the solar cycle (see solar flux F10.7-index in Table 1). There were no significant geomagnetic variations or intense solar flares.

4. Background conditions

The Earth's ionosphere is sensible to different kind of phenomena (Davis, 1965; Cander, 2019). It is important to distinguish between the ionospheric disturbances of different origin. During and before the days corresponding to the two considered seismic events, Space Weather conditions were rather quiet. No intense solar flare occurred. The geomagnetic conditions were characterized with the Dst-index minimum values of -18 nT and -24 nT on September 8, 2021, and September 19, 2022, respectively. These values indicate very weak perturbations, but no geomagnetic storm that could provide ionospheric scintillations occurred.

The two main sources of gravity waves are the passage of solar terminator and solar eclipse (Laštovička, 2006). Therefore, another background factor to consider is the solar terminator passage which can be a source of the ionospheric wave-like irregularities (Somsikov, 2011). Figure 3 illustrates the conditions during the two considered days. The first event occurred near the time of terminator passage. In the second case, the event occurred at daytime.

Table 1. EQ parameters.

Event	Epicenter (lat, lon), °	M_w	LT	Duration of rupture (MRF)*, s	Dept, km	Surface rupture length, km	Rupture directivity	Fault mechanism	Geomagnetic storm and/or solar flare	F10.7-index, s.f.u.
8- Sep-2021	16.7553N, 99.9533W	7.1	20:47	12.5	15	30	NE	Thrust	None	101.9
19-Sep-2022	18.2377N, 103.269W	7.7	13:05	80	12.1	80	NW	Thrust	None	129.1

*MRF – Moment Rate Function.

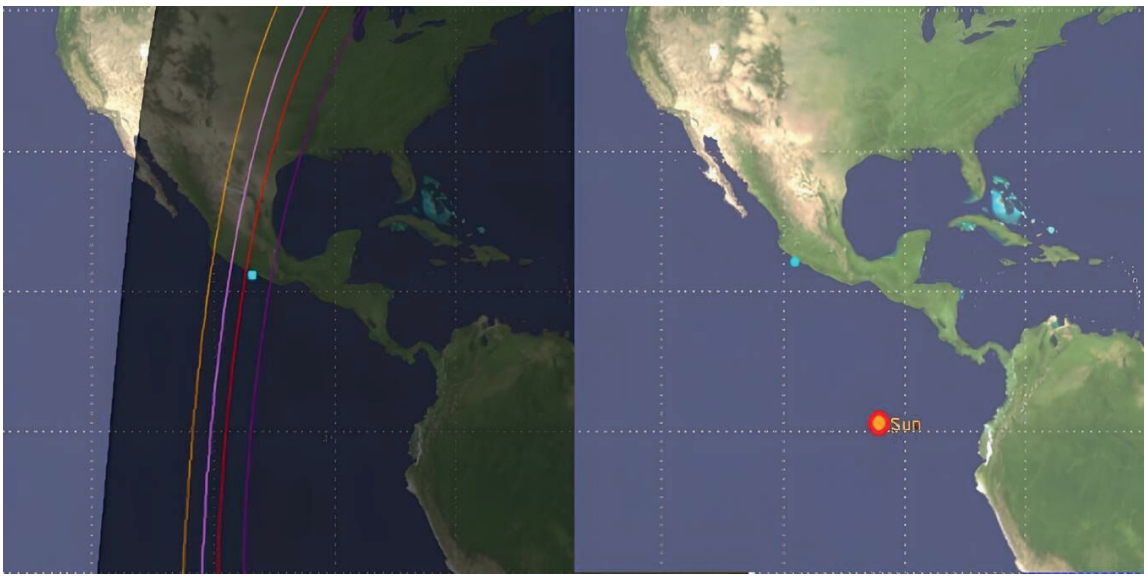

Figure 3. Terminator conditions at the moments of EQ: September 8, 2021 (left) and September 19, 2022 (right). EQ epicenters are marked with light blue points. Yellow, rose, red and violet lines stand for the terminator positions at 100, 150, 200 and 300 km above the Earth's surface. The position of the Sun at its zenith is marked by the red circle.

4. Results and discussion

4.1. September 8, 2021

The EQ of September 8, 2021, was an evening event. Therefore, it was possible that the solar terminator motion generated acoustic-gravity waves that in turn could cause the ionospheric disturbances (Somsikov, 2011; Edemskiy and Yasyukevich, 2018; Borchevkina and Karpov, 2018; Grzesiak and Świątek, 2012; Figueiredo *et al.*, 2018) with the signatures similar to disturbances that potentially resulted from the EQ. The possible effects of solar terminator could manifest themselves as a front of wave-packet TEC disturbances in the ionosphere stretched along the terminator line (Somsikov, 2011) before or after the terminator's movement at the ionospheric heights (Borchevkina & Karpov, 2018). No such effects were detected on September 8th over Mexico. Probably, the terminator did not provoke effects, or the front of the disturbance passed over the center of Mexico before the considered time interval.

The form of the compression-rarefaction wave (N-form) related to shockwaves is characteristic for the dI response to a powerful earthquake (Astafyeva, 2019; Gautam *et al.*, 2018; He & Heki, 2017; Afraimovich, 2001; Afraimovich *et al.*, 2013). The considered EQ occurred at 01:47 UT (20:47 LT) and was followed by the aftershocks. The most intense were M_w 5.2 and M_w 5.0 at 02:18 and 02:58 UT, correspondingly.

The N-form in (10-20)dI variations was detected at individual LoSs with the approximate period of ~30 min, which correspond to the medium-scale ionospheric irregularities triggered by atmospheric gravity waves (Hocke & Schlegel, 1996; Astafyeva, 2019) that in turn were caused by the surface displacement during the EQ. In some cases, the inverse N-form (И) was observed. The amplitude of registered disturbances depended on the LoS configuration and varied between 0.1 and 0.2 TECU. No such

signatures in the (10-20)dI time series were present at the same time on other days. Therefore the detected disturbances cannot be a result of the multipath effect. For the same reason they may not be associated with the waves of orographic origin. Figure 4 illustrates the observed picture.

Some of disturbances were detected far from the EQ epicenter: more than 1000 km. According to Astafyeva (2009), this is not impossible. We estimated the "horizontal" speed of the detected disturbances departing from the rough assumption that they began to propagate just after the EQ. This is the common assumption for CID studies (Liu *et al.*, 2023; Sripathi *et al.*, 2020; Gautam *et al.*, 2018; Liu *et al.*, 2010; Astafyeva *et al.*, 2009; Afraimovich *et al.*, 2006). The CIDs with very high speeds were discarded as not probable. The rest of the disturbances propagated with speeds close to three values: ~1200 m/s, ~540 m/s and ~260 m/s in all directions except eastward (Figure 4b). Furthermore, the disturbances characterized with the too low speeds were associated with the time and coordinates of the two aftershocks which resulted into the most of them propagating with no direction preference and with the speed close to ~120 m/s. Figures 4b and 4c show the sub-ionospheric point positions at which the mentioned ionospheric disturbances were revealed.

To sum up, the dI responses were registered at individual satellite-receiver ray paths after the EQ of M_w 7.1. During disturbances, the filtered TEC variations exceeded the level of the background fluctuations and were not repeated on other days. The amplitudes of dI fluctuations varied between 0.1 and 0.2 TECU. The first of them were detected 13 min after the main shock. The form of the dI curve, the time and distance at which the disturbances were detected allow us to relate them to the effects of gravity waves generated by the EQ and, possibly, its two aftershocks.

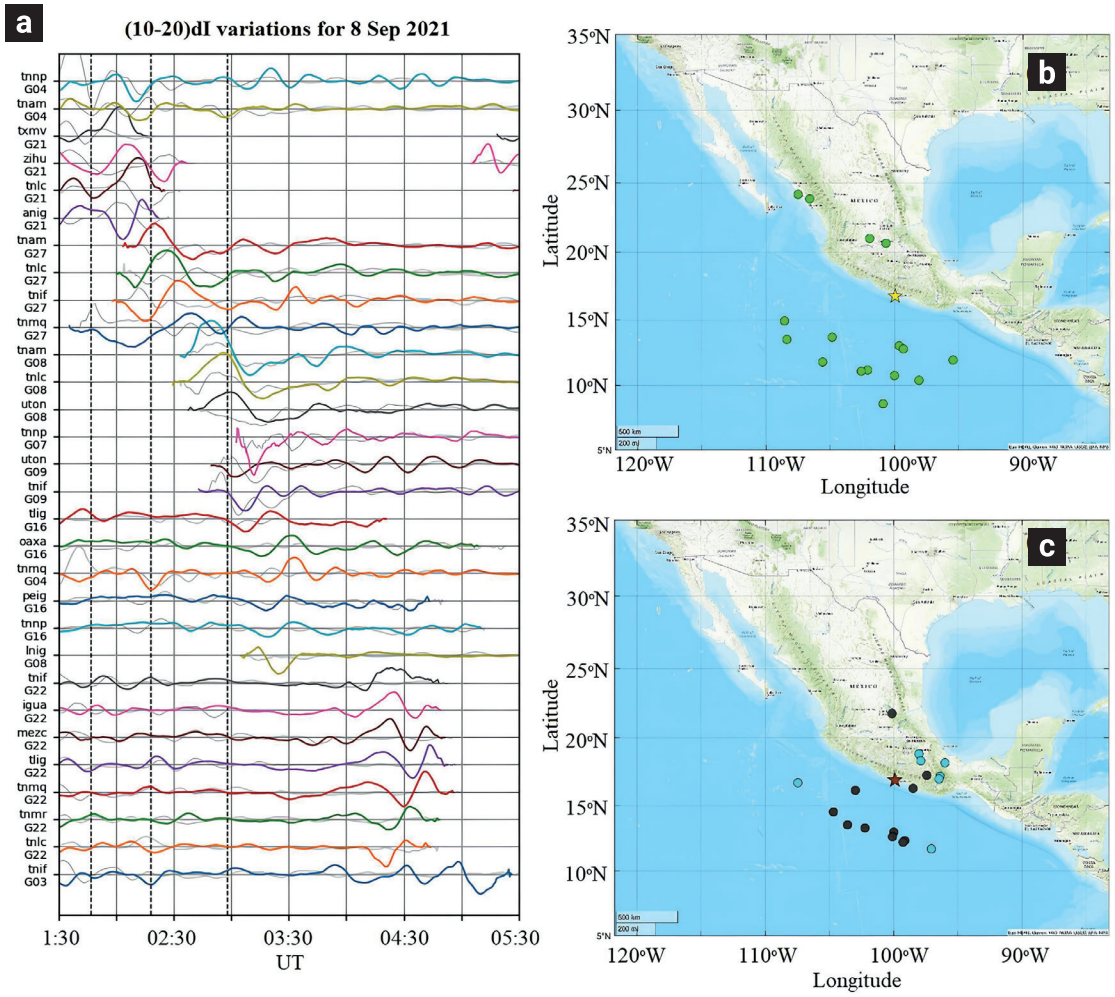

Figure 4. (a) (10-20)dI time series at individual LoSs on September 8, 2021. The receiver-satellite pairs are indicated at the Y-axis. Y-axis unit is 0.2 TECU. X-axis unit is 30 min. The dotted vertical lines mark the moments of EQ and its two aftershocks. Colored curves stand for the EQ day variations and gray curves for the same variations on the previous day. (b) Position of sub-ionospheric points for disturbances associated with the main shock and (c) with aftershocks. Magenta points in panel "c" stand for the possible CIDs after the first aftershock and grey points after the second aftershock. Yellow star marks EQ epicenter, claret star marks aftershock epicenters.

4.2. September 19, 2022

The analysis of dI variations after the EQ of September 19, 2022, allowed us revealing two types of ionospheric irregularities that may be related to the acoustic-gravity waves originated from the EQ. Figure 5a illustrates the N-form disturbances detected in (2-10)dI variations. Their amplitudes exceeded the level of the background variations and varied in a wide range of (0.1-1.1 TECU) depending on the LoS. No such variations were observed on other days. At some LoSs, the N-form was inversed (И) or transformed into V- or M-form. The period of detected disturbances was about 15 min. The applied centered moving average window size and the period imply that these were the small-scale disturbances.

Figure 5b shows positions of sub-ionospheric points for the chosen LoSs after the main shock. The "horizontal" speeds of most of disturbances were close to the value of ~323 m/s. The faster disturbances with speeds close to ~650 and ~880 m/s were registered as well. The distribution of disturbances was mostly southward and northward from the epicenter. Some of disturbances from Figure 5a may be related to the aftershock M_w 5.3 that occurred at 19:30 UT. These propagated northward and eastward from the aftershock epicenter with speeds close to ~320 m/s and ~110 m/s (Figure 5c).

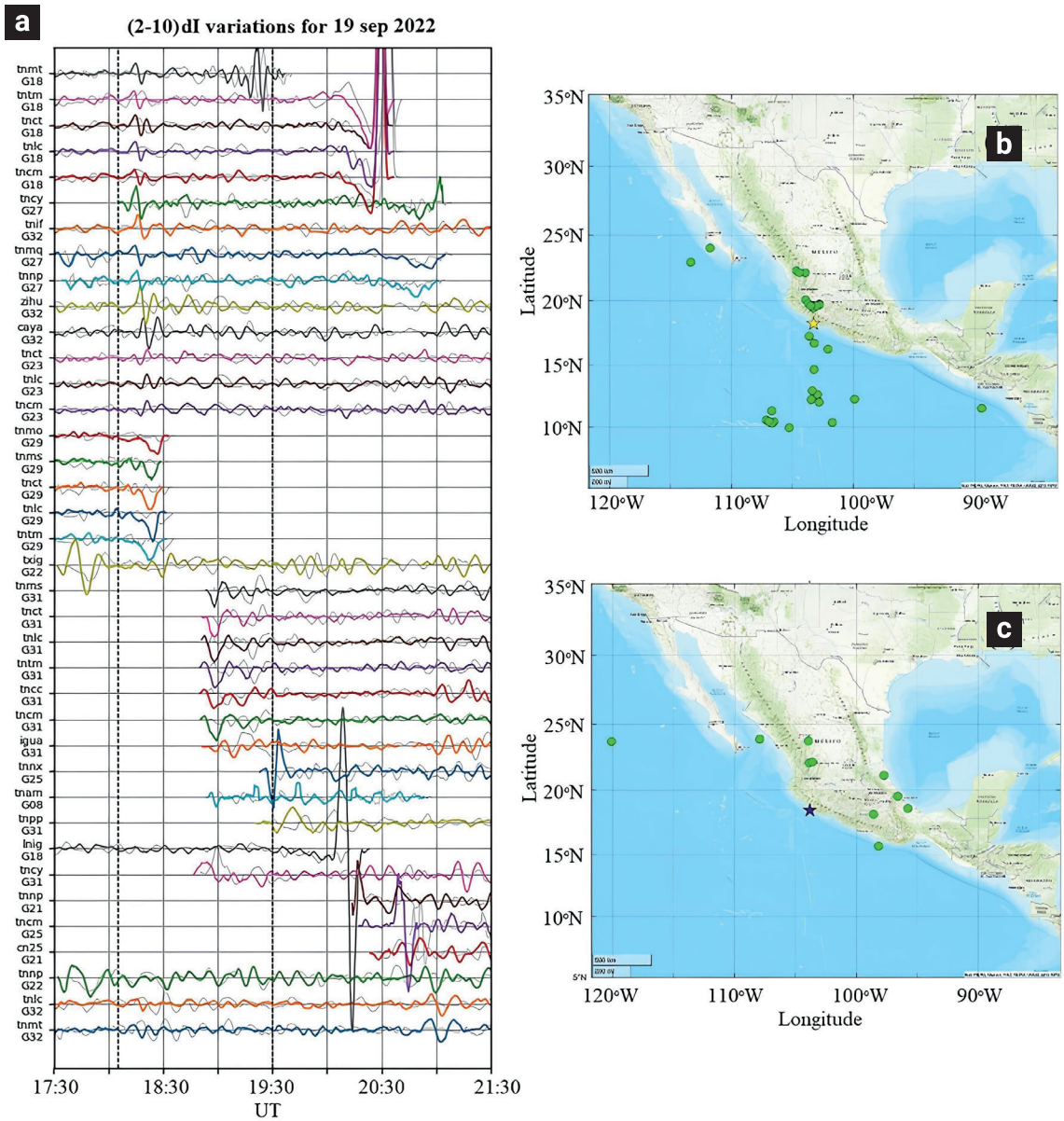

Figure 5. (a) The same as in Figure 4, but for (2-10)dIv series at the individual LoSs on September 19, 2022. (b) Position of the sub-ionospheric points for disturbances associated with the main shock and (c) aftershock. Yellow star marks EQ epicenter and claret star marks the aftershock epicenter.

Moreover, the N- and И-form were also detected at some LoSs in (10-20)dI variations. Figure 6 illustrates the picture. These may be associated with the medium scale disturbances related to gravity waves. Their amplitudes were ~(0.1-0.2) TECU and the period was about 30 min. The first signatures were detected ~25 min after the EQ. The estimated speeds were mostly close to the values of ~320 m/s and ~158 m/s. The speed of ~533 m/s was also detected at two LoSs. Some individual responses may be associated with the aftershock and be characterized with the speed of ~230 m/s.

To sum up, the multi-scale ionospheric disturbances were formed after the EQ M_w 7.7 and its aftershock. Perhaps, the presence of two scales of CIDs was due to the higher electron concentration during the daytime hours if compare to the nighttime EQ of September 8, 2021. The higher EQ magnitude may also play a role. The small-scale disturbances propagated southward and northward from the epicenter. The medium-scale disturbances propagated in different directions. In general, the picture of disturbances was rather complex.

4.3. Possibility of tsunami-induced disturbances.

Atmospheric gravity waves can be also induced by a tsunami (Peltier and Hines 1976; Artu *et al.*, 2005; Jin *et al.*, 2019). According to the bulletins of National Mareographic Service of Mexico, after the EQ of September 8, 2021, the largest amplitude of 95 cm in sea level deviation from the astronomical tide forecast was registered at the mareographic station located ~8 km in a straight line from the epicenter: the decrease by~60 cm followed by the increase by ~35 cm. Other seven mareographic stations at the Pacific Ocean coast of Mexico registered much less amplitudes (10-40 cm) [SMN, 2021]. After EQ of September 19, 2022, the maximum wave height of ~1.7 m was registered at the coastal station located ~140 km northwestward from the epicenter, four other stations gave 1 m, 0.90m, 0.69 m and 0.41 m amplitudes at each of them [SMN, 2022]. In addition, according to (Zaytsev *et al.*, 2023), the open-ocean station of Deep-ocean Assessment and Reporting of Tsunamis (DART) (Rabinovich & Eblé, 2015) located

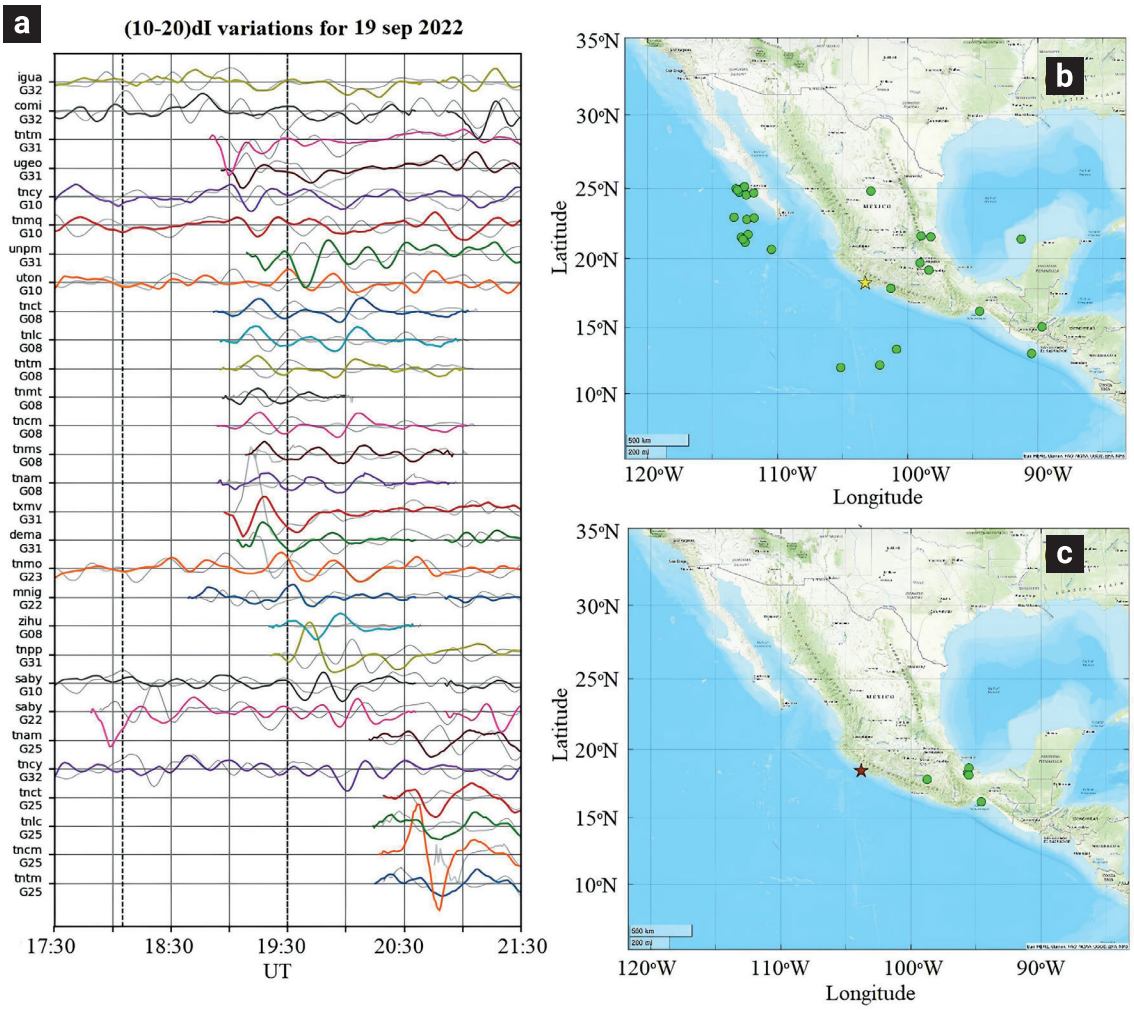

Figure 6. The same as in Figure 4, but for September 19, 2022.

at a distance of ~884 km from the EQ epicenter registered the maximum wave height of 7.4 cm.

It is fair to expect that the associated ionospheric disturbances (if formed) would follow the tsunami front (Lognonné, 2009). In the first case (September 8, 2021), it would be some near semi-circular front propagating away from the coast, but no similar ionospheric disturbance propagation was registered. The difficulty is that the signatures of ionospheric disturbances caused by EQ and tsunami can be similar (Artu *et al.*, 2005; Jin *et al.*, 2019). Five of "grey points" in Figure 4c, seem to be "aligned" in the ocean. However, two considerations prevent us to associate them clearly to tsunami. First, there are also the similar "grey points" over the continent. Second, the amplitudes and the form of TEC deviations are quite similar for all detected disturbances and no specific type within some time-interval is distinguished.

In the second case (September 19, 2022), tsunami energy radiation pattern in the ocean was directed like a "searchlight" oriented normally to the mainland coast (Zaytsev *et al.*, 2023). Considering this specific feature, the possible ionospheric response would have a similar propagation pattern, but no such disturbances were registered in the filtered TEC series (Figure 5c and Figure 6c).

Maybe, these negative results are due to the combination of factors that could include the insufficient sea level deviation amplitudes (in general, not at one coastal station) or tsunami propagation not long enough to generate sufficient upward gravity wave and others factors. For the definitive results it is also needed a better LoSs coverage in the region to have more sub-ionopheric points for the analysis.

5. Conclusions

Two recent EQs of $M_w > 7.0$ that occurred in the south of Mexico in 2021 and 2022 were studied. Wave responses in the filtered slant TEC time series were revealed after both seismic events at individual satellite-receiver ray paths. These variations exceeded the level of background fluctuations and were not repeated on other days. The form of the dI curve, the time and distance at which the disturbances were detected allowed us to relate them to the effects of acoustic and gravity waves in the atmosphere generated by the EQs and as a possibility by their intense aftershocks.

The ionospheric response to the EQ of M_w 7.1 on September 8, 2021 was detected as N- and И-form medium-scale disturbances with the period of ~30 min. Their amplitudes varied between 0.1 and 0.2 TECU. Our results show that CIDs triggered by the EQ propagated at different speeds close to the values of ~1200 m/s, ~540 m/s and ~260 m/s in all directions except eastward. Those that may be associated with the two intense aftershocks propagated with the speeds close to ~120 m/s.

The ionospheric response of two types were revealed after the EQ of M_w 7.7 on September 19, 2022. First, there were detected the N-, И-, V- and M-form small-scale disturbances characterized with a ~15 min period and amplitudes within (0.1-1.1) TECU. Furthermore, there were detected the N- and И-form medium scale disturbances with the period of ~30 min and amplitudes between 0.1 and 0.2 TECU. Their speeds were mostly close to the values of ~320 m/s and ~158 m/s. Some individual responses with the speed of ~230 m/s may be associated with the aftershock.

For both considered events no clear indication of the ionospheric response to tsunami was found. For the definitive results a better LoSs coverage in the region is needed.

To conclude, the epicenter location, depth, focal mechanism, season, and Space Weather background conditions were rather similar for both events. The difference in the responses may be attributed to a combination of factors such as local time and EQ magnitude. This is the preliminary conclusion made for the Mexican region as more statistics is needed.

6. Acknowledgements

LANCE acknowledges partial support from CONACyT-AEM, Grant 2017-01-292684 and CONACyT LN-315829. A. Melgarejo-Morales express their gratitude to CONAHCyT.

The authors thank TLALOCNet at Servicio de Geodesia Satelital (Cabral-Cano *et al.*, 2018) and the Servicio Sismológico Nacional (Pérez-Campos *et al.*, 2018; **https://doi.org/10.21766/SSNMX/SN/MX),** both hosted at the Instituto de Geofísica, Universidad Nacional Autónoma de México, and in particular to Luis Salazar-Tlaczani at the Instituto de Geofísica, Universidad Nacional Autónoma de México (UNAM) with support from UNAM-PAPIIT project IN107321, and the National Science Foundation grant 2025104 to the College of New Jersey, and also the GAGE facility operated by UNAVCO. The data was processed with the SIMuRG tools (Yasukevich *et al.*, 2020).

The OMNI data (Dst and F10.7 indices) were obtained from the GSFC/SPDF OMNIWeb interface at **https://omniweb.gsfc.nasa.gov** (accessed on 09 September 2023). The authors thank Dr. Kalishin (AARI) for the opportunity to calculate the solar terminator positions with use of "Solar Terminator" software which is freely available by following the link **https://www.sciesmex.unam.mx/integrantes/maria-sergeeva/solarterminator/.**

The authors would like to thank the Editor and the anonymous reviewers for their contributing comments.

7. References

Afraimovich, E. L., Astafieva, E. I., & Kirushkin, V. V. (2006).

Localization of the source of ionospheric disturbance generated during an earthquake. *International Journal of Geomagnetism and Aeronomy*, 6(2), 1-13.

Afraimovich, E.L., Astafyeva, E.I., Demyanov, V.V., Edemskiy, I.K., Gavrilyuk, N.S., Ishin, A.B., Kosogorov, E.A., Leonovich, L.A., Lesyuta, O.S., Palamartchouk, K.S., Perevalova, N. P., Polyakova, A. S., Smolkov, G. Y., Voeykov, S. V., Yasyukevich, Y, V., & Zhivetiev, I. V. (2013). A review of GPS/GLONASS studies of the ionospheric response to natural and anthropogenic processes and phenomena. *J. Space Weather Space Clim.* 3. doi: **https://doi.org/10.1051/swsc/2013049**

Afraimovich, E.L., Perevalova, N.P., Plotnikov, A.V, & Uralov, A.M. (2001). The shock-acoustic waves generated by earthquakes. *Annales Geophysicae*. 19(4), 395–409. doi: **https://doi.org/10.5194/angeo-19-395-2001**

Artru J., Ducic, V., Kanamori, H., Lognonné, P., & Murakami, M. (2005). Ionospheric detection of gravity waves induced by tsunamis, Geophysical Journal International, 160(3), 840-848. doi: **https://doi.org/10.1111/j.1365-246X.2005.02552.x**

Astafyeva, E. (2019). Ionospheric detection of natural hazards. *Reviews of Geophysics*, 57(4), 1265–1288. doi: **https://doi.org/10.1029/2019RG000668**

Astafyeva, E., Heki, K., Kiryushkin, V., Afraimovich, E., & Shalimov, S. (2009). Two mode long-distance propagation of coseismic ionosphere disturbances. Journal of Geophysical Research, 114(A10). doi: **https://doi.org/10.1029/2008JA013853**

Borchevkina, O.P., & Karpov, I.V. (2018). Observations of variations in total electron content in the solar terminator region in the ionosphere, Sovrem. *Probl. Distantsionnogo Zondirovaniya Zemli Kosmosa*, 15(1), 299–305. doi: **https://doi.org/10.21046/2070-7401-2018-15-1-299-305**

Borchevkina, O.P., Adamson, S.O., & Dyakov, Y.A. *et al.* (2021). The influence of tropospheric processes on disturbances in the D and E ionospheric layers. *Atmosphere*, 12(9), 1116. doi: **https://doi.org/10.3390/atmos12091116**

Bravo, M., Benavente, R., Foppiano, A., Urra, B., & Ovalle, E. (2022). Traveling Ionospheric Disturbances observed over South America after lithospheric events: 2010–2020. *Journal of Geophysical Research: Space Physics*, 127(4). doi: **https://doi.org/10.1029/2021JA030060**

Cabral-Cano, E., Pérez-Campos, X., Márquez-Azúa, B., Sergeeva, M.A., Salazar-Tlaczan, L., DeMets, C., Adams, D., Galetzka, J., Hodgkinson, K., Feaux, K., Serra, Y. L., Mattioli, G. S., & Miller, M. (2018). TLALOCNet: A Continuous GPS-Met Backbone in Mexico for Seismotectonic, and Atmospheric Research. *Seismological Research Letters*. 89(2A), 373–381. doi: **https://doi.org/10.1785/0220170190**

Calais, E. & Minster, B. (1995). GPS detection of ionospheric perturbations following the January 17, 1994, Northridge Earthquake. *Geophysical Research Letters*. 22(9), 1045-1048. doi: **https://doi.org/10.1029/95GL00168**

Cander, L.R. (2019) *Ionospheric Space Weather*. Springer Geophysics. Springer, Cham. doi: **https://doi.org/10.1007/978-3-319-99331-7**

Davies, K. (1965). *Ionospheric radio propagation*. US Department of Commerce, National Bureau of Standards.

Davies, K., & Baker, D. M. (1965). Ionospheric effects observed around the time of the Alaskan earthquake of March 28, 1964. *Journal of Geophysical Research*, 70(9), 2251– 2253. doi: **https://doi.org/10.1029/JZ070i009p02251**

Ducic, V., Artru, J., & Longnonne, P. (2003). Ionospheric remote sensing of the Denali Earthquake Rayleigh surface wave. *Geophysical Research Letters*, 30(18). doi: **https://doi.org/10.1029/2003GL017812**

Edemskiy, I. K., & Yasyukevich, A. S. (2018). Observing wave packets generated by solar terminator in TEC during typhoons. *Solar-Terrestrial Physics*, 4(2), 33-40. doi: **https://doi.org/10.12737/stp-42201806**

Figueiredo, C. A. O. B., Takahashi, H., Wrasse, C. M., Otsuka, Y., Shiokawa, K., & Barros, D. (2018). Medium-scale traveling ionospheric disturbances observed by detrended total electron content maps over Brazil. *Journal of Geophysical Research: Space Physics*, 123(3), 2215-2227. doi: **https://doi.org/10.1002/2017JA025021**

Gautam, P. K., Chauhan, V., Sathyaseelan, R., Kumar, N., & Pappachen, J. P. (2018). Co-seismic ionospheric GPS-TEC disturbances from different source characteristic earthquakes in the Himalaya and the adjoining regions. *NRIAG Journal of Astronomy and Geophysics*. 7(2), 237-246. doi: **https://doi.org/10.1016/j.nrjag.2018.05.009**

Golubkov, G.V., Adamson, S.O., & Borchevkina, O.P. *et al.* (2022). Coupling of Ionospheric Disturbances with Dynamic Processes in the Troposphere. *Russian Journal of Physical Chemistry B*, 16(3), 508–530. doi: **https://doi.org/10.1134/S1990793122030058**

Gonzalez-Esparza, J. A., Sergeeva, M. A., Corona-Romero, P., Mejia-Ambriz, J.C., Gonzalez, L.X., V. De la Luz, Aguilar-Rodriguez, E., Rodriguez, M., & Romero-Hernández, E. (2018). *Space weather* events, hurricanes, and earthquakes in Mexico in September 2017. Space Weather, 16(12), 2038–2051. doi: **https://doi.org/10.1029/2018SW001995**

Grzesiak, M., & Świątek, A. (2012). Solar terminator-related ionosphere derived from GPS TEC measurements: a case study. *Acta Geophysica*, 60, 1224-1235. doi: **https://doi.org/10.2478/s11600-011-0048-7**

He, L., & Heki, K. (2017). Ionospheric anomalies immediately before M_w7.0–8.0 earthquakes, *J. Geophys. Res. Space Physics*, 122, 8659–8678. doi:10.1002/2017JA024012

Heki, K., & Ping, J. (2005). Directivity and apparent velocity of the coseismic ionospheric disturbances observed with a dense GPS array. *Earth and Planetary Science Letters*, 236(3-4), 845-855. doi: **https://doi.org/10.1016/j.epsl.2005.06.010**

Hocke, K. & Schlegel, K. (1996). A review of atmospheric gravity waves and travelling ionospheric disturbances: 1982-1995. *Annales Geophysicae*, 14, 917–940. doi: **https://doi.org/10.1007/s00585-996-0917-6**

Iglesias, A., Singh, S.K., Castro-Artola, O., Pérez-Campos, X., Corona-Fernandez, R.D. Santoyo, M.A., Espíndola, V.H., Arroyo, D. & Franco, S.I. (2022). A Source Study of the M_w7.0 Acapulco, Mexico, Earthquake of 8 September 2021. *Seismological Research Letters*, 93(6), 3205–3218. doi: **https://doi.org/10.1785/0220220124**

Jin, S., Jin, R., Liu, X., Jin, S., Jin, R., & Liu, X. (2019). Tsunami Ionospheric Disturbances. En A. Shuanggen Jin, R. Jin, X. Liu (Eds.), *GNSS Atmospheric Seismology: Theory, Observations and Modeling* (pp.211-244) Springer Singapore. doi: **https://doi.org/10.1007/978-981-10-3178-6_12**

Jin, S., Occhipinti, G., & Jin, R. (2015). GNSS ionospheric seismology: Recent observation evidences and characteristics. *Earth-Science Reviews*, 147, 54-64. doi: **https://doi.org/10.1016/j.earscirev.2015.05.003**

Kazimirovsky, E.S., Kokourov, V.D., & Vergasova, G.V. (2006). Dynamical climatology of the upper mesosphere, lower thermosphere and ionosphere. *Surveys Geophysics*. 27, 211–255. doi: **https://doi.org/10.1007/s10712-005-3819-3**

Kelly, M.C. (2009). *The Earth's Ionosphere: Plasma Physics and Electrodynamics*, (2a ed.) Academic Press (Elsevier), San Diego, CA USA.

Kong, J., Yao, Y., & Zhou, C. *et al.* (2018). Tridimensional reconstruction of the Co-Seismic Ionospheric Disturbance around the time of 2015 Nepal earthquake. *Journal of Geodesy*, 92, 1255–1266. doi: **https://doi.org/10.1007/s00190-018-1117-3**

Laštovička, J. (2006). Forcing of the ionosphere by waves from below. *Journal of Atmospheric and Solar-Terrestrial Physics*, 68(3-5), 479-497. **https://doi.org/10.1016/j.jastp.2005.01.018**

Liu, C., Lay, T., Bai, Y., He, P., & Xiong, X. (2023). Coseismic Slip Model of the 19 September 2022 M w 7.6 Michoacán, Mexico, Earthquake: A Quasi-Repeat of the 1973 M_w 7.6 Rupture. *The Seismic Record*, 3(2), 57-68. doi: **https://doi.org/10.1785/0320220042**

Liu, J. Y., Tsai, H. F., Lin, C. H., Kamogawa, M., Chen, Y. I., Lin, C. H., Huang, B. S., Yu, S. B., & Yeh, Y. H. (2010). Coseismic ionospheric disturbances triggered by the Chi-Chi earthquake. *Journal of Geophysical Research*, 115(A8), A08303, doi: **https://doi.org/10.1029/2009JA014943**

Lognonné, P. (2009). Seismic waves from atmospheric sources and atmospheric/ionospheric signatures of seismic waves. En A. Le Pichon, A., Blanc, E., Hauchecorne, A. (Eds) *Infrasound Monitoring for Atmospheric Studies*, (pp. 281-304). Springer, Dordrecht. doi: **https://doi.org/10.1007/978-1-4020-9508-5_10**

Lognonné, P., Artru, J., Garcia, R., Crespon, F., Ducic, V., Jeansou, E., Occhipinti, G., Helbert, J., Moreaux, G., & Godet, P. E. (2006). Ground-based GPS imaging of ionospheric post-seismic signal, *Planetary and Space Science*, 54(5), 528-540. doi: **https://doi.org/10.1016/j.pss.2005.10.021**

Melgarejo-Morales, A., Vazquez-Becerra, G.E., Millan-Almaraz, J. R., Martinez-Felix, C.A., & Munawar, S. (2023). Applying support vector machine (SVM) using GPS-TEC and Space Weather parameters to distinguish ionospheric disturbances possibly related to earthquakes. *Advances in Space Research*. 72(10), 4420-4434. doi: **https://doi.org/10.1016/j.asr.2023.08.028**

Oikonomou, C., Haralambous, H., Pulinets, S., Khadka, A., Paudel, S. R., Barta, V., Muslim, B., Kourtidis, K., Karagioras, A., & Inyurt, S. (2020). Investigation of Pre-Earthquake Ionospheric and Atmospheric Disturbances for Three Large Earthquakes in Mexico. *Geosciences*, 11(1), 16. doi: **https://doi.org/10.3390/geosciences11010016**

Peltier, W.R., Hines, C.O. (1976). On the possible detection of tsunamis by a monitoring of the ionosphere. *Journal of Geophysical Research*, 81(12), 1995-2000, doi: **https://doi.org/10.1029/JC081i012p01995**

Perevalova, N.P., & Ishin, A.B. (2011) Effects of tropical cyclones in the ionosphere from data of sounding by GPS signals. *Izvestiya Atmospheric and Oceanic Physics*, 47, 1072–1083. doi: **https://doi.org/10.1134/S000143381109012X**

Perevalova, N.P., Sankov, V. A., Astafyeva, E.I., & Zhupityaeva, A.S. (2014). Threshold magnitude for Ionospheric TEC response to earthquakes. *Journal of Atmospheric and Solar-Terrestrial Physics*, 108, 77-90. doi: **https://doi.org/10.1016/j.jastp.2013.12.014**

Perevalova, N.P., Shestakov, N.V., Voeykov, S.V., Takahashi, H., & Guojie, M. (2015). Ionospheric disturbances in the vicinity of the Chelyabinsk meteoroid explosive disruption as inferred from dense GPS observations. *Geophysical Research Letters*, 42(16), 6535–6543. doi: **https://doi.org/10.1002/2015GL064792**

Pérez-Campos, X., Espíndola, V.H., Pérez, J., Estrada, J.A., Monroy, C.C., Bello, D., González-López, A., Gonzalez Avila, D., Contreras Ruiz Esparza, M.G., Maldonado, R., & *et al.* (2018). The Mexican National Seismological Service: An Overview. Seismological Research Letters, 89(2A), 318-323. doi: **https://doi.org/10.1785/0220170186**

Rabinovich, A.B., & Eblé, M.C. (2015). Deep ocean measurements of tsunami waves. *Pure and Applied Geophysics*. 172, 3281–3312. doi: **https://doi.org/10.1007/s00024-015-1058-1**

Ramírez-Rojas, A., Flores-Márquez, E.L., Vargas, C.A. (2023). Visibility Graph Analysis of the Seismic Activity of Three Areas of the Cocos Plate Mexican Subduction Where the Last Three Large Earthquakes (M > 7) Occurred in 2017 and 2022. *Entropy*, 25(5), 799. doi :**https://doi.org/10.3390/e25050799**

Rolland, L., Vergnolle, M., Nocquet, J.-M., Sladen, A., Dessa, J.X. Tavakoli, F., Nankali, H.R. & Cappa, F. (2013). Discriminating the tectonic and non-tectonic contributions in the ionospheric signature of the 2011, M_w7.1, dip-slip Van earthquake, Eastern Turkey. *Geophysical Research Letters*. 40(11), 2518-2522, doi: **https://doi.org/10.1002/grl.50544**

Sergeeva, M.A., Demyanov, V.V., Maltseva, O.A., Mokhnatkin, A., Rodriguez-Martinez, M., Gutierrez, R., Vesnin, A.M., Gatica-Acevedo, V.J., Gonzalez-Esparza, J.A., Fedorov, M.E., Ishina, T. V., Pazos, M., Gonzalez, L.X., Corona-Romero, P., Mejia-Ambriz, J.C., Gonzalez-Aviles, J.J., Aguilar-Rodriguez, E., Cabral-Cano, E., Mendoza, B., Romero-Hernandez, E., Caraballo, R., & Orrala-Legorreta, I.D. (2021). *Assessment of Morelian Meteoroid Impact on Mexican Environment. Atmosphere*. 12, 185. doi: **https://doi.org/10.3390/atmos12020185**

Sergeeva, M.A., Maltseva, O.A., Vesnin, A.M., Blagoveshchensky, D.V., Gatica-Acevedo, V.J., Gonzalez-Esparza, J.A., Chernov, A.G., Orrala-Legorreta, I.D., Melgarejo-Morales, A., & Gonzalez, L.X.; *et al.* (2023). Solar Flare Effects Observed over Mexico during 30–31 March 2022.

Remote Sens. 15, 397. doi: **https://doi.org/10.3390/rs15020397**

Shi, K., Guo, J., & Liu, X. *et al.* (2020). Seismo-ionospheric anomalies associated with M_w 7.8 Nepal earthquake on 2015 April 25 from CMONOC GPS data. Geosciences Journal 24, 391–406. doi: **https://doi.org/10.1007/s12303-019-0038-3**

Singh, S.K., Iglesias, A., Arroyo, D., Pérez-Campos X., Ordaz, M., Mendoza, C., Corona-Fernández, R.D., Rivera, L.V., Espíndola, H., González-Ávila, D., Martínez-López, R., Castro-Artola, O., Santoyo, M.A., & S. I. Franco; A Seismological Study of the Michoacán-Colima, Mexico, Earthquake of 19 September 2022 (M_w7.6). *Geofísica Internacional*, 62(2) 445-465. doi: **https://doi.org/10.22201/igeof.2954436xe.2023.62.2.1453**

Servicio Mareográfico Nacional. (2021). Reporte preliminar: registro en las estaciones del Servicio Mareográfico Nacional del tsunami producido por el sismo de magnitud 7.1 ocurrido en Acapulco, Guerrero, *Boletín del Servicio Mareográfico Nacional del Instituto de Geofísica de la Universidad Nacional Autónoma de México*, 1-15.

Servicio Mareográfico Nacional. (2022). Reporte final: Registro en las estaciones del Servicio Mareográfico Nacional del tsunami producido por el sismo de magnitud 7.7 ocurrido en Michoacán, *Boletín del Servicio Mareográfico Nacional del Instituto de Geofísica de la Universidad Nacional Autónoma de México*, 1-18

Somsikov, V.M. (2011). Solar terminator and dynamic phenomena in the atmosphere: A review. Geomagn. *Aeron*. 51, 707-719. doi: **https://doi.org/10.1134/S0016793211060168**

Sripathi, S., Singh, R., Tiwari, P., & Kumar, M. R. (2020). On the co-seismic ionospheric disturbances (CIDs) in the rapid run ionosonde observations over Allahabad following M_w 7.8 Nepal Earthquake on April 25, 2015. *Journal of Geophysical Research: Space Physics*. 125. doi: **https://doi.org/10.1029/2019JA027001**

Servicio Sismológico Nacional (2021). *Reporte especial. Sismo del 7 de septiembre de 2021, guerrero (M 7.1)*, Servicio Sismológico Nacional, Instituto de Geofísica, UNAM, México. **http://www.ssn.unam.mx/sismicidad/reportes-especiales/2021/SSNMX_rep_esp_20210907_Guerrero_M71.pdf**

Servicio Sismológico Nacional (2022). Reporte especial. Sismo del 19 de septiembre de 2022, Michoacán (M 7.7), 2022. Servicio Sismológico Nacional, Instituto de Geofísica, UNAM, México. **http://www.ssn.unam.mx/sismicidad/reportes-especiales/2022/SSNMX_rep_esp_20220919_Michoacan_M74.pdf**

Yasyukevich, Y.V., Kiselev, A.V., Zhivetiev, I.V., Edemskiy, I.K., Syrovatskii, S.V., Maletckii, B.M., & Vesnin, A.M. (2020). SIMuRG: System for Ionosphere Monitoring and Research from GNSS. *GPS Solut.* 24, 69. doi: **https://doi.org/10.1007/s10291-020-00983-2**

Zaytsev, O., Tsukanova, E., Rabinovich, A.B., Thomson, R.E. (2023). The Michoacán Tsunami of 19 September 2022 on the Coast of Mexico: Observations, Spectral Properties and Modelling. *Water*. 15, 164. doi: **https://doi.org/10.3390/w15010164**

Zhang, Y., Liu, X., Guo, J., Shi, K., Zhou, M., & Wang, F. (2021). Co-Seismic Ionospheric Disturbance with Alaska Strike-Slip M_w 7.9 Earthquake on 23 January 2018 Monitored by GPS. *Atmosphere*. 12, 83. doi: **https://doi.org/10.3390/atmos12010083**